DEVELOPMENT OF A HYDROGEN COMBUSTOR FOR A MICROFABRICATED GAS TURBINE ENGINE

A. Mehra, I. A. Waitz
Gas Turbine Laboratory, Department of Aeronautics and Astronautics
Massachusetts Institute of Technology
Cambridge, MA 02139

ABSTRACT

As part of an effort to develop a new generation of micro heat engines, a program is underway to fabricate a gas turbine engine capable of producing 50W of electrical power in a package less than one cubic centimeter in volume. This paper focuses on the combustor for such an engine, specifically describing the design, fabrication and testing of a first-ever hydrogen combustor micromachined from silicon. Complete with a fuel manifold and injector holes, the combustion chamber measuring less than 0.07 cm^3 in volume has been successfully demonstrated to provide exit temperatures up to 1800K. The combustor efficiencies were found to be in the range of 40%-60% due to large heat loss to the test mount. The device has been experimentally tested at elevated temperatures for over fifteen hours, demonstrating the satisfactory performance of silicon in such environments. Combined with a materials study that shows that the performance of a silicon microcombustor will not be oxidation limited, these results are a significant step towards establishing the viability of building a micro gas turbine engine using silicon microfabrication techniques.

INTRODUCTION

Recent advances in the field of microfabrication have opened the possibility of building a micro gas turbine engine. By using the material properties of silicon and the precision obtainable from microfabrication technology, a micro gas turbine engine could produce tens of watts of power while weighing only a few grams, and being a few millimeters in dimension. Such a device would represent a significant advance in compact electrical power sources by providing over ten times the energy and power density of the best batteries available today. Besides power generation, microengines could become an enabling technology for numerous other applications such as boundary layer and circulation control, micro air vehicle propulsion, micro refrigeration, micro rocket engines, automotive fuel pumps, and mobile power units.

A feasibility study, preliminary design and performance estimates of a device requiring 7 grams of jet fuel per hour and producing 10-100 Watts of electrical power have been presented by Epstein *et al.* **(1)** and Groshenry **(2)**. This device is shown in Figure 1. Since several micro heat engine applications require the conversion of chemical energy into fluid and thermal power, it is necessary to develop combustion strategies suitable for use in these miniature devices. The challenges and preliminary design of such a combustor were described by Waitz *et al.* **(3)**, along with the results for premixed hydrogen combustion in a macrofabricated steel rig measuring 130 mm^3 in volume. This paper extends these results. Non-premixed hydrogen-air combustion is demonstrated in a first-of-its-kind combustor that is micromachined from silicon, and has an integral fuel manifold and injector holes. The results of a materials study are also presented to establish the viability of silicon as a suitable material for a micro gas turbine engine.

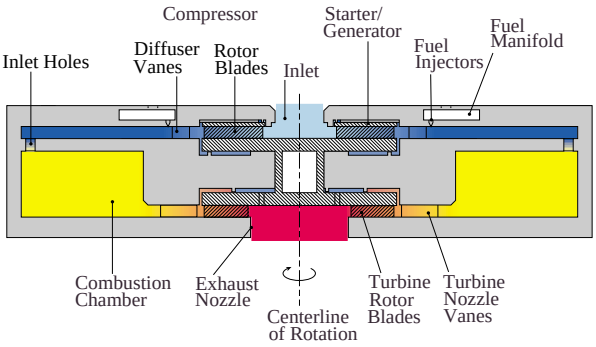

Figure 1: Baseline design of the MIT micro gas turbine engine and electrical generator.

HYDROGEN-AIR MICROCOMBUSTORS

Before describing the fabrication and testing of the microcombustor, we briefly review the primary challenges and the proposed combustion strategies.

Overview of Microcombustion Technology

The design and operation of a combustor at the micro scale is primarily limited by the following:

1. *Shorter residence time for mixing and combustion:* Since combustor residence time approximately scales with combustor volume and compressor pressure ratio **(4)**, the residence time in a low pressure, low volume, geometrically scaled down microcombustor may be a tenth to a hundredth of that in a conventional large scale gas turbine combustor. This imposes constraints on the time available for fuel mixing and chemical reactions[1].
2. *High heat loss at the micro scale:* The surface area-to-volume ratio of the microcombustor is 500 m^{-1}, compared to 3-5 m^{-1} for a large scale combustor. Thus, high heat transfer losses may prevent the attainment of typical large scale combustor efficiencies which are in excess of 99.9%, and may also affect fuel flammability limits due to flame quenching.

[1]Compared to a conventional sized gas turbine with pressure ratios in excess of 30:1, the pressure ratio for the baseline microengine is only 4:1.

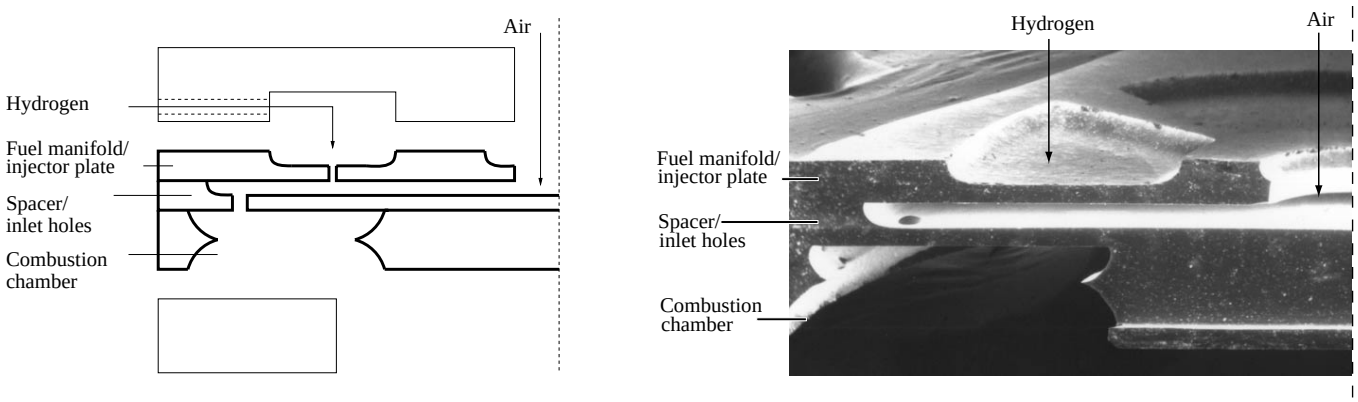

Figure 2: Schematic and SEM cross-section of half of the combustor, showing the fuel manifold, injectors, and air flow path.

In response to these challenges, the design of the microcombustor is based on the following strategies:

1. Relative to the size of the engine, the size of the combustor was increased by a factor of 40 to increase the flow residence time.
2. The fuel was introduced at approximately 50 injector-hole diameters upstream of the combustor inlet holes to facilitate fuel-air mixing.
3. Hydrogen was chosen as a fuel since it has wider flammability limits, and an order of magnitude lower chemical reaction time than hydrocarbon fuels[2].

In keeping with these concepts, the design, fabrication and testing of a micromachined silicon combustor has been completed. This is presented in the following sections.

Design of the Microcombustor

The schematic of the microcombustor assembly is shown in Figure 2. The microfabricated portion consists of a stack of three silicon wafers housing the fuel manifold and injectors, the combustor inlet holes, and the combustion chamber. The chamber is an annular region 1 mm in height, with a volume of 66 mm^3, and an inner and outer diameter of 5 mm and 10 mm respectively. The axial length of the combustor was chosen in accordance with the computational fluid dynamics (CFD) predictions for the minimum volume necessary for complete combustion at atmospheric pressure. It also facilitates the fabrication of the entire combustion chamber from a single 1 mm thick wafer.

The fuel injector size and spacing was based on semi-empirical models for normal jet injection and mixing to satisfy lateral spreading and penetration requirements. The final device consists of a total of 76 30μm diameter injector holes equally spaced at a radius of 3 mm.

The overall combustor dimensions were set by the preliminary design studies completed by Epstein *et al.* **(1)**. The size and number of combustor inlet holes was chosen to eliminate the upstream propagation of a flame into the compressor exit flow path.

[2]While initial efforts have primarily concentrated on the use of hydrogen, a program for the use of hydrocarbon-air combustion is also currently underway **(3)**.

Fabrication Process

The three stack fusion-bonded assembly required a total of five masks and six deep etches. The fabrication process for each of the wafers involved the following steps:

1. Photolithography: A 10μm coating of resist was used to pattern the top surface of the wafer with the appropriate fuel manifold, spacer plate or combustion chamber geometry.
2. Isotropic Deep Reactive-Ion Etching (DRIE), **(5)**: Dry chemistry employing an SF_6 plasma was used to etch the 200μm fuel manifold and spacer plate. Half of the 1000μm deep combustion chamber was also isotropically etched, the double-sided etching technique being employed to minimize the run-out in the side walls of the combustor[3].
3. Patterning bottom side: After coating 10μm of resist, infra-red alignment was used to expose the bottom side of the three wafers to pattern the corresponding fuel injectors, combustor inlet holes, or combustion chamber geometry.
4. Anisotropic DRIE: Finally, a time multiplexed inductively coupled plasma of SF_6 and C_4F_8 was used to anisotropically etch the 200μm deep fuel injectors and combustor inlet holes in the top two wafers of the stack. (The other side of the combustion chamber wafer was isotropically etched.)

Following the completion of the processing on the three individual wafers, the wafers were RCA cleaned, and aligned bonded using a Electronic Visions aligner. The bonding was completed in two steps - the first and second wafers were bonded first; the stack was then annealed, RCA cleaned, and finally bonded to the third wafer. Post-bond annealing was carried out in an inert ambient for one hour at 1100°C. The 1.8 mm thick wafer-stack was finally die-sawed to obtain thirteen out of the possible sixteen die on the 100 mm wafer.

A cross section of the completed stack showing the fuel manifold, injector holes and fluid flow paths is shown in Figure 2. Individual scanning electron micrographs of each of the wafers are shown in Figures 3-5.

[3]Since none of the features required parallel side walls, isotropic etching was chosen to minimize process time.

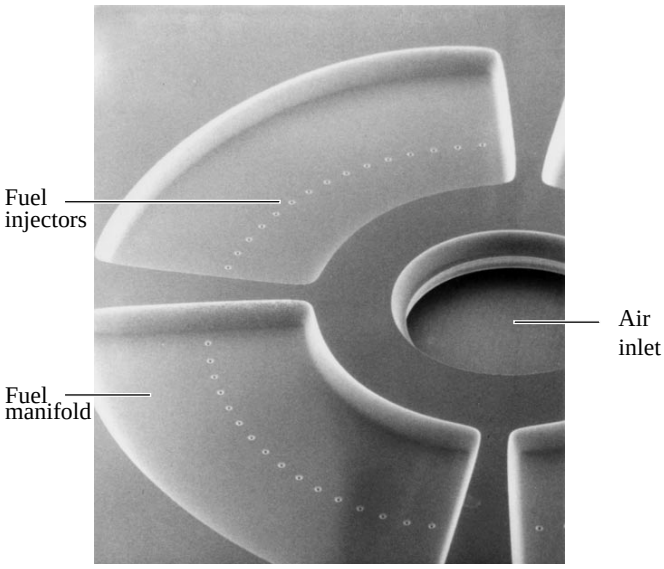

Figure 3: SEM of the fuel manifold, showing the ring of 76 30μm fuel injector holes.

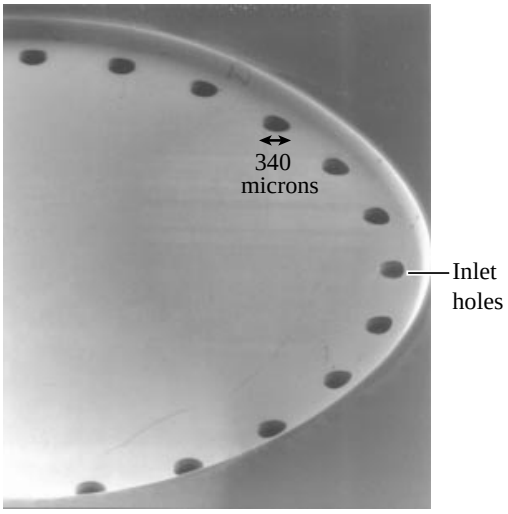

Figure 4: Isotropically etched spacer plate, showing the 24 340μm combustor inlet holes at r=4.5 mm.

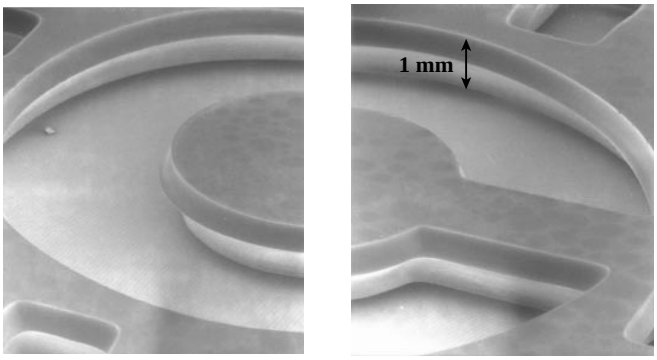

Figure 5: Isotropically etched, 1 mm high annular combustion chamber, with an inner and outer diameter of 5 mm and 10 mm respectively.

Experimental Tests

Apparatus

A schematic of the experimental test rig is shown in Figure 6. The microfabricated structure was clamped between invar plates whose thermal expansion coefficients were chosen to match that of silicon. The invar plates also housed the macro-fluidic connections for the air and hydrogen feeds, along with inlet and exit thermocouples. Type K thermocouples were employed for temperature measurements. However, because of large temperature gradients along the length of the wire, an error analysis for the thermal conductivity, radiative emissivity and calibration drifts predicted that the uncertainty in temperature measurements would be up to ±120K **(6)**. While these uncertainty bounds were considered acceptable to establish the onset of combustion, efforts are currently underway to incorporate non-intrusive optical techniques to improve temperature diagnostics.

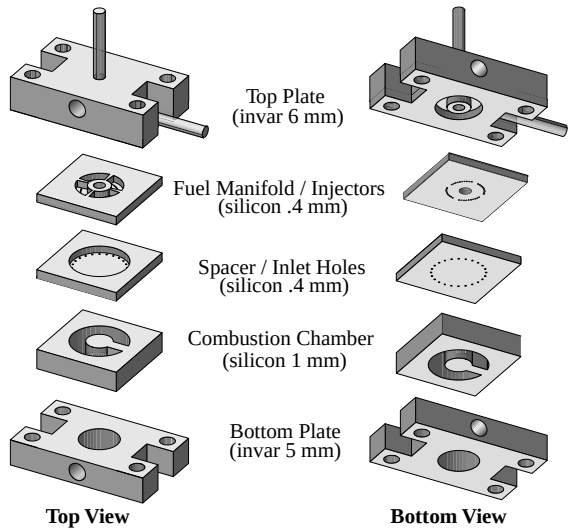

Figure 6: A schematic of the microcombustor test rig (Wafer thicknesses are exaggerated for illustrative effect).

Results

Atmospheric test results were obtained for premixed and non-premixed hydrogen-air combustion over most of the flammability range. The combustor operating parameters under stoichiometric conditions are shown in Table 1. The

Air mass flow $\dot{m}_a$ (g/sec)	.045
Fuel mass flow $\dot{m}_f$ (g/sec)	1.3×10^{-3}
Flow residence time (sec)	1.7×10^{-3}
Average wall temperature (K)	900
Exit temperature (K)	1800
Fluid power (Watts)	70
Combustor efficiency	44%
Space heating rate (MW/m^3/atm)	$\sim$ 1000

Table 1: Microcombustor operating parameters for stoichiometric hydrogen combustion at 1 atm. (premixed).

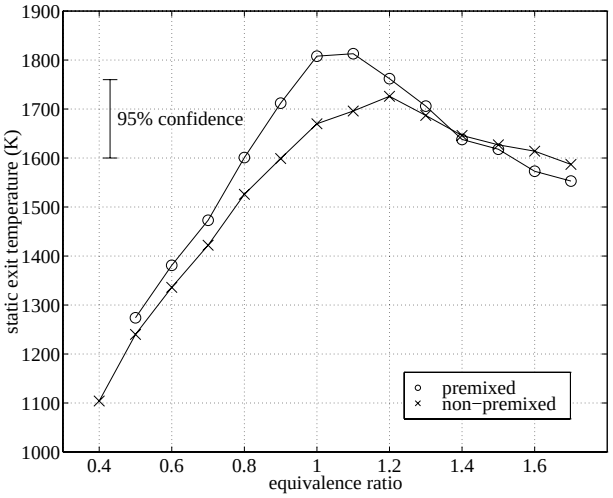

Figure 7: Microcombustor test results, showing exit temperatures up to 1800K.

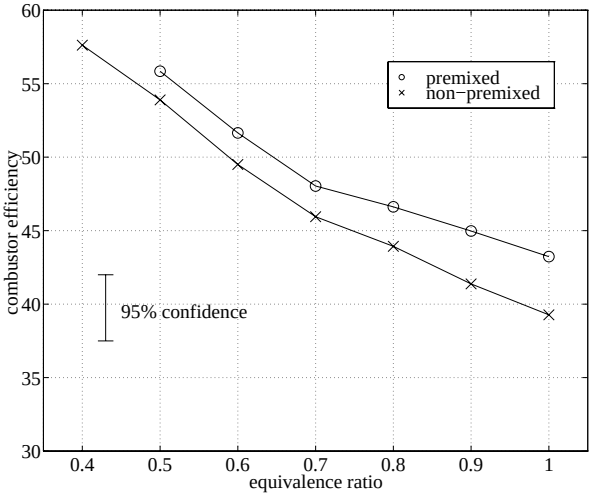

Figure 8: Efficiency measurements for the microcombustor.

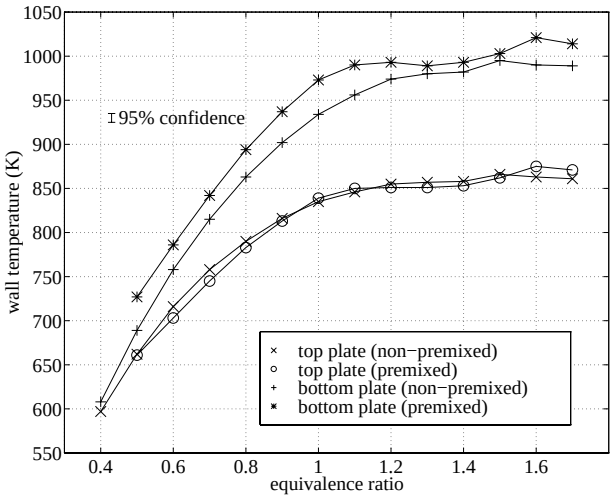

Figure 9: Microcombustor test results, showing wall temperatures well below the melting point of silicon.

corrected results for the exit temperatures are also shown in Figure 7, indicating satisfactory attainment of exit temperatures up to 1800K. As expected, the peak exit temperatures occurred slightly beyond stoichiometric conditions. For the premixed case however, the exit temperatures were approximately 100K higher, suggesting incomplete fuel-air mixing upstream of the combustor. This is attributed to a slight mis-alignment of the wafers during bonding, which effectively reduced the fuel mixing length on one side of the combustor.

Even though desired turbine inlet temperatures were obtained, poor thermal isolation of the rig resulted in excessive heat loss. As defined in Eq. (1), and shown in Figure 8, the combustor efficiency was found to be in the range of 40%-60%.

$$\eta_{comb} = \frac{(\dot{m}_a + \dot{m}_f)C_pT_{exit} - \dot{m}_aC_pT_{inlet}}{\dot{m}_f h_f} \qquad (1)$$

The losses correlated well with a simple heat transfer model for the heat loss through top and bottom invar plates, suggesting that incomplete combustion was not the source of the inefficiency. Thus, the *combustion* efficiency is predicted to have been close to unity, even though the combustor efficiency was significantly lower. Currently, efforts are underway to improve the thermal insulation of the rig, and increase the combustor efficiency into a more desirable range.

As shown in Figure 9, the walls of the combustor were found to be relatively cooler than the combustion gases. This is attributed to the excessive heat loss out of the combustor, which allows the structure to operate below the melting point of silicon even as the combustor gas temperature is in excess of 2000K. While improved thermal insulation is expected to raise the wall temperature, the reduced equivalence ratios required to achieve desired turbine inlet temperatures would also correspondingly lower the chamber temperature. This suggests that the combustor walls shall continue to operate at relatively cooler temperatures, even if thermal insulation and combustor efficiency are further increased.

Overall, while high pressure testing and improved temperature diagnostics still need to be employed, the combustor has been successfully tested to provide turbine inlet temperatures of up to 1800K for over fifteen hours. As shown in Figure 10, the structure maintains its structural integrity, and shows no visible damage. These results demonstrate the satisfactory performance of a micromachined silicon combustor for applications in a micro heat engine.

OXIDATION, MATERIALS STUDY

As shown in Figure 10, post-combustion examination of the silicon microcombustor indicated oxidation patterns around the structure and the combustion inlet holes. A materials study was consequently undertaken to further quantify the effects of silicon oxidation in a combustion environment.

Oxidation Tests

As part of an oxidation study, a combustor plate consisting of "finger-like" structures with sizes between $20\mu m \times 500\mu m \times 450\mu m$ and $1600\mu m \times 2000\mu m \times 450\mu m$ was fabricated and tested inside the combustor. Shown in Figure 11, the plate was fabricated by anisotropically etching through a single $450\mu m$ silicon wafer.

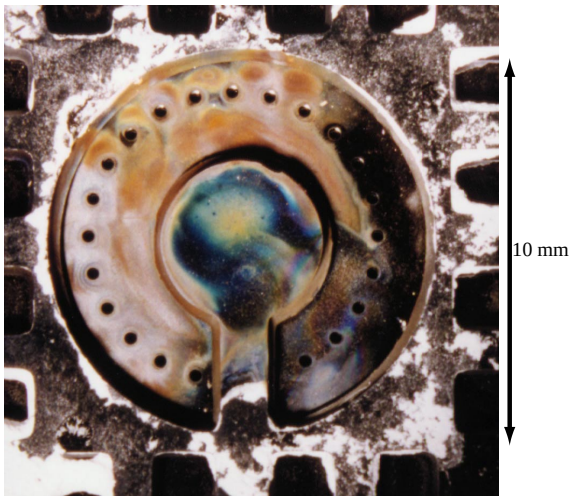

Figure 10: *Post-combustion appearance of the rig after 15 hours of testing at T_{exit} ~1800K. While the oxidation patterns are apparent, the structure shows no visible damage.*

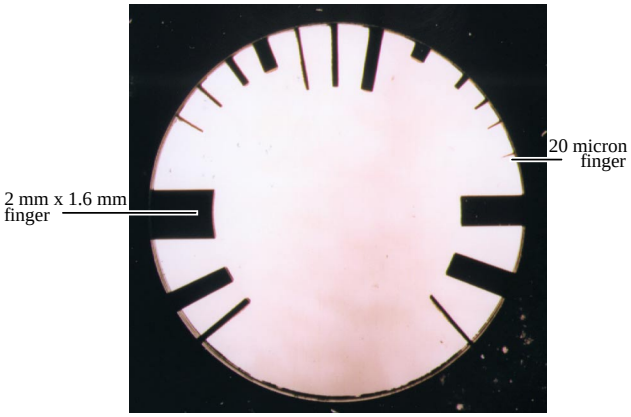

Figure 11: *Photograph of the silicon combustor plate with "finger-like" structures (sizes range between 20μm × 500μm × 450μm and 1600μm × 2000μm × 450μm).*

The structure was exposed to a combustion environment for over 8 hours at atmospheric pressures and flow temperatures in excess of 2000K[4]. Depending on the size and aspect ratio of the fingers, and hence the temperature at which they equilibrated, the fingers grew between 1μm and 10μm of amorphous oxide. This suggests that the "active-oxidation" of silicon is not an overriding concern for this particular application, the oxide thickness being the same order of magnitude as that predicted by the Deal-Grove passive oxidation model (**7**).

The thinnest of the fingers however, measuring 20μm × 500μm × 450μm, grew crystalline oxide. This is shown in Figure 12. While the thinnest finger is expected to have experienced the highest tip and surface temperatures, the specific criteria causing the growth of crystalline versus amorphous oxide on the walls of the microcombustor have not yet been established.

Although atmospheric pressure testing failed to reveal any limiting failure mechanisms, elevated pressure testing of the fingered combustor plate identified creep to be the failure mechanism for silicon in microcombustion environments. As shown in Figure 13, at fluid temperatures in excess of 2200K, and at higher stress levels resulting from pressures of approximately 3 atm., several of the fingers were found to creep. The location of the point where the different fingers began to be bend correlated well with a two-dimensional heat transfer model for the temperature distributions along the length of the fingers. This suggests that creep failure of the fingers followed the brittle-to-plastic transition of silicon, occurring at approximately 900K.

[4]The overall wall temperature was once again in the range of a 1000K.

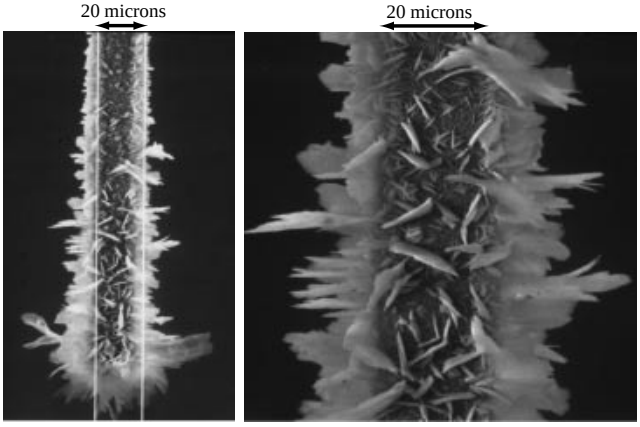

Figure 12: *Crystalline oxide growth on the 20μm × 500μm × 450μm finger.*

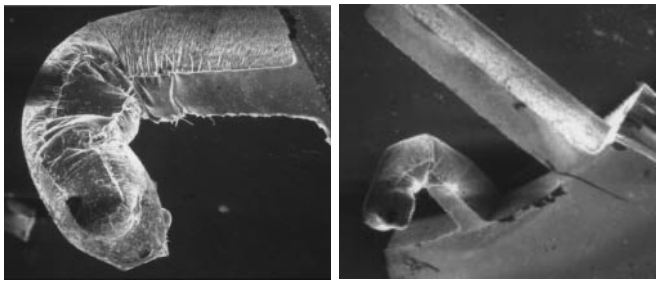

Figure 13: *SEM of a 200μm × 450μm × 2000μm structure after combustion, showing creep limited performance of silicon.*

Turbine Vane Tests

Although atmospheric tests showed that oxidation was not a limiting factor in the operation of a silicon microcombustor, the impact of higher Mach number (~ 1) and associated higher heat transfer rates in a typical turbine flow environment is unknown. While the effects on the critically stressed rotor cannot be assessed in the absence of a spinning structure, a set of 150μm high turbine nozzle guide vanes was exposed to the combustor exhaust in order to examine the effects of oxidation in a highly erosive, high temperature and pressure, supersonic flow environment. Figure 14 shows before and after pictures of a turbine stator vane following a five hour exposure to combustion exhaust at 1800K and 2.5 atm., and at a mass flow of 0.1 g/sec. While "pitting" and erosion is visible on the blade surface,

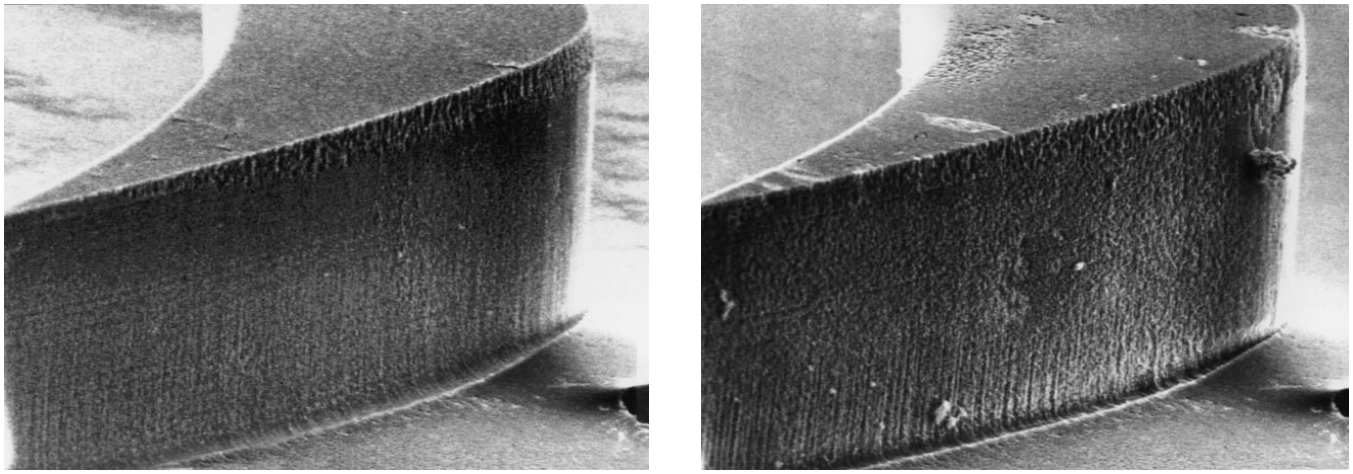

Figure 14: Before and after pictures of the vanes following a 5 hour exposure to combustion exhaust gases at 1800K, Mach number $\sim$ 1. Although the blades exhibit minor erosion and "pitting", they maintain their structural integrity. (The blades are $150\mu m$ *high).*

the vanes appeared to be minimally damaged; the increase in throat area resulting in no more than a 2% change in mass flow. This establishes the survivability of a static vane structure in a high pressure and temperature, and high Mach number flow environment.

SUMMARY AND CONCLUSIONS

As part of an effort to develop a micro gas turbine engine using silicon microfabrication technologies, the design, fabrication and testing of a first-ever hydrogen combustor micromachined from silicon has been reported. Complete with a fuel manifold and injector holes, the combustion chamber measuring less than 0.07 cm^3 in volume has been successfully demonstrated to sustain premixed and non-premixed hydrogen combustion, providing exit temperatures of up to 1800K. While the performance of silicon was found to be creep limited at elevated pressures and temperatures in excess of 2200K, the combustor has been experimentally tested at elevated temperatures for over fifteen hours, thereby demonstrating the satisfactory performance of silicon in such harsh environments. Combined with the results of an oxidation study which showed that the performance of a silicon microcombustor will not be oxidation limited, these results are an important step towards establishing the viability of building a new generation of micro heat engines using silicon microfabrication technology.

ACKNOWLEDGMENTS

We would first like to recognize and thank Professor Alan H. Epstein for his conception and pursuit of the MIT microengine project, and for being a constant source of encouragement and inspiration. We acknowledge the support of the fabrication team comprising Professor Martin A. Schmidt, Professor Stephen D. Senturia, Dr. Arturo A. Ayon, Dr. Reza Ghodissi, and C. C. Lin, for training and provision of etch recipes. We are also grateful to all the other members of the MIT microengine team for support during various stages of this research, especially Dr. Gautam Gauba and Yang-Sheng Tzeng for their research on temperature diagnostics for microcombustion phenomenon. Finally, special thanks to Diana Park for all the help with the graphics.

This work was largely supported by the Army Research Office through Grant DAAHO4-95-1-0093, with Dr. Richard Paur as program manager. All devices were fabricated at the MIT Microsystems Technological Laboratories.

Nomenclature

T	Temperature (K)
C_p	Specific heat at constant pressure (kJ/kg-K)
h_f	Fuel heating value (kJ/kg)
$\dot{m}_a$	Mass flow rate of air (kg/sec)
$\dot{m}_f$	Mass flow rate of fuel (kg/sec)
η_{comb}	Combustor efficiency

References

[1] Epstein *et al.*, *"Micro-Heat Engines, Gas Turbines, and Rocket Engines"*, presented at the 28^{th} AIAA Fluid Dynamics Conference, 1997.

[2] Groshenry, C., *"Preliminary Study of a Micro-Gas Turbine Engine"*, S.M. Thesis, Massachusetts Institute of Technology, 1995.

[3] Waitz, I. A., Gauba, G., Tzeng, Y-S., *"Combustors for Micro-Gas Turbine Engines"*, Proceedings of the ASME Aerospace Division, AD-Vol. 52, 1996.

[4] Kerrebrock, J. L., *"Aircraft Engines and Gas Turbines"*, 2nd ed., MIT Press, 1992.

[5] Ayon *et al.*, *"Characterization of a Time Multiplexed Inductively Coupled Plasma Etcher, Part 1"*, submitted to the Journal of Vacuum Science and Technology, 1997.

[6] Tzeng., Y-S., *"An Investigation of Microcombustion Thermal Phenomenon"*, S.M. Thesis, Massachusetts Institute of Technology, 1997.

[7] Deal, B. E., Grove, A. S., *"General Relationship for the Thermal Oxidation of Silicon"*, Journal of Applied Physics, Vol. 36., p. 3770., 1965.

Keyword List:

Combustor efficiency
Deep Reactive Ion Etching
Fuel injector
Fuel manifold
Fusion bonding
Gas turbine engine
Hydrogen-air combustion
Microcombustor
Micro heat engine
Silicon oxidation
Silicon creep
Turbine inlet temperature